

## Periodic Forcing of Inhibition-Stabilized Networks: Nonlinear Resonances and Phase-Amplitude Coupling

**Romain Veltz**

*romain.veltz@inria.fr*

*Howard Hughes Medical Institute, Salk Institute for Biological Studies, La Jolla, CA 92037, and INRIA, Sophia Antipolis Mediterrane, 06902 France*

**Terrence J. Sejnowski**

*sejnowski@salk.edu*

*Howard Hughes Medical Institute, Salk Institute for Biological Studies, La Jolla, CA 92037, U.S.A., and Division of Biological Sciences, University of California San Diego, La Jolla, CA 92093 U.S.A.*

**Inhibition-stabilized networks (ISNs) are neural architectures with strong positive feedback among pyramidal neurons balanced by strong negative feedback from inhibitory interneurons, a circuit element found in the hippocampus and the primary visual cortex. In their working regime, ISNs produce damped oscillations in the  $\gamma$ -range in response to inputs to the inhibitory population. In order to understand the properties of interconnected ISNs, we investigated periodic forcing of ISNs. We show that ISNs can be excited over a range of frequencies and derive properties of the resonance peaks. In particular, we studied the phase-locked solutions, the torus solutions, and the resonance peaks. Periodically forced ISNs respond with (possibly multistable) phase-locked activity, whereas networks with sustained intrinsic oscillations respond more dynamically to periodic inputs with tori. Hence, the dynamics are surprisingly rich, and phase effects alone do not adequately describe the network response. This strengthens the importance of phase-amplitude coupling as opposed to phase-phase coupling in providing multiple frequencies for multiplexing and routing information.**

### 1 Introduction ---

Oscillatory rhythms of neuronal populations are ubiquitous in the brain (see Buzsaki, 2004, for a review), but their functions are not yet established (Sejnowski & Paulsen, 2006). Gamma oscillations in the 30–80 Hz frequency band (Bartos, Vida, & Jonas, 2007) have been implicated in attention and memory (Yamamoto, Suh, Takeuchi, & Tonegawa, 2014), in coding information, and in communication between brain areas (Buzsaki & Chrobak, 1995; Bichot, Rossi, & Desimone, 2005; Ray & Maunsell, 2011; Womelsdorf

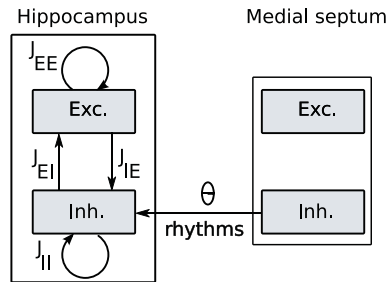


Figure 1: Entrainment of theta activity in hippocampus by rhythmic inhibition of inhibitory interneurons.

et al., 2012; Igarashi, Lu, Colgin, Moser, & Moser, 2014) and are abnormal in pathologies such as schizophrenia (Lewis, Hashimoto, & Volk, 2005), autism (Wright et al., 2012), and Parkinson's disease (Hemptonne et al., 2013).

Gamma frequency oscillations are often coupled with oscillations at lower frequencies (Jensen & Colgin, 2007). For example, oscillating inputs to the hippocampus from the medial septum are in the theta frequency range (4–8 Hz). CA1 neurons in hippocampus also receive inputs from the medial entorhinal cortex in the high gamma frequency range (60–80 Hz) and inputs from the CA3 neuron in the low gamma frequency range (30–60 Hz) (Colgin et al., 2009). When neural networks in these different regions are coupled, there is an interplay between oscillations that are internally generated and those that arise from external inputs.

Analyzing these networks theoretically is difficult (Borisyyuk, Borisyyuk, Khibnik, & Roose, 1995), even at the scale of neural populations, because the interplay of multiple frequencies may lead to chaotic behavior (Newhouse, Ruelle, & Takens, 1978). Large-scale network models of these oscillations also have large numbers of parameters, which are difficult to analyze (Vierling-Claassen, Siekmeier, Stufflebeam, & Kopell, 2008). However, this analysis can be more easily undertaken in models with fewer parameters and the intrinsic working regimes of the different neural populations are known. A good example of this is Tsodyks, Skaggs, Sejnowski, and McNoughton (1997), which analyzed a neural model of hippocampal circuits forced by inputs from the medial septum (see Figure 1). This network consisted of two populations of interconnected neurons, excitatory and inhibitory, such that when the inhibitory connections are removed, the remaining excitatory network is unstable. Network stability was maintained by strong inhibitory network connections, putting the network into a dynamical regime called an inhibition stabilized network (ISN). Recently, ISNs have been used to model the cortical visual area (Murphy & Miller, 2009; Ozeki, Finn, Schaffer, Miller, & Ferster, 2009; Jadi & Sejnowski, 2014a, 2014b; Rubin, Van Hooser, & Miller, 2015), and they can also be found in studies where

the ISN regime is not explicitly invoked (Kang, Shelley, Henrie, & Shapley, 2010; Akam, Oren, Mantoan, Ferenczi, & Kullmann, 2012).

Two properties of these ISNs make them especially interesting. First, increasing the direct external input to the inhibitory interneurons causes the interneurons paradoxically to decrease their firing rates, and, second, the ISN operating regime supports intrinsic gamma oscillations.

The main objective of this article is to understand the amplification of gamma rhythms of networks driven by periodic external inputs when the gamma rhythm are generated resonantly within the circuitry of the network. To this end, we focus on the ISN, which, we will see, can be understood as damped oscillators. There are several reasons to perform this analysis in addition to the considerations already identified:

1. An extension of Tsodyks et al. (1997) is to assume that the hippocampus contains interconnected ISNs. As a first step toward the study of such networks, we can consider a feedforward chain of two ISNs and the even simpler case where the last ISN of the chain is periodically forced (by the first ISN)
2. ISNs have been shown to be relevant for the description of the local circuitry of V1 (see the experimental papers by Ozeki et al., 2009, and Rubin et al., 2015): interconnected ISNs would then be adequate for the study of center/surround interactions.
3. It has been shown recently (Akam et al., 2012) that a firing rate model of CA3 neuron with sustained oscillations can be used to fit the phase response curve (PRC) of carbachol-induced oscillations as well as optogenetic stimulation. The PRC is a tool (Ermentrout & Terman, 2010) valid far from a bifurcation point. This suggests that the PRC is inadequate for the study of forced ISNs where phase-amplitude coupling may arise (Aronson, Ermentrout, & Kopell, 1990).

Periodic forcing of neural oscillators is a well-studied paradigm, but most papers are not applicable to periodic forcing of ISN because they assume, first, that the oscillations are sustained (see, e.g., Neu, 1979; Ermentrout, 1981); second, that the forcing amplitude is small compared to the amplitude of the network oscillations; and the third concerns the forcing frequency  $\omega_F$ , which is off resonance with an intrinsic frequency  $\omega_H$ , that is, it is not related by a rational number. As a consequence, resonance effects are ignored (see, e.g., Hoppensteadt & Izhikevich, 1997).

One notable exception to the first assumption is Aronson et al. (1990), although resonance conditions were not addressed. These above assumptions naturally lead to the limited description of phase-locked (PL) solutions that are  $\omega_F$ -periodic solutions with constant amplitude. Hence, the only variable in these solutions is the relative phase between the forcing and the output, which is assumed to encode information. This scheme is called phase-phase coupling in the literature.

Here, we go beyond a phase description and look at how the amplitude of the response is affected by nonlinear resonance effects. The resonance effect in which a network with intrinsic frequency  $\omega_H$  displays a maximum in the amplitude of the response when the forcing frequency  $\omega_F$  is close to  $\omega_H$  has been known for some time. It was used recently in experiments (Cardin et al., 2009) to investigate the neural mechanism responsible for gamma oscillations in the barrel cortex. It has been used in Akam and Kullmann (2010) to show how to multiplex information and also in Paik and Glaser (2010) to show how the visual cortex can adjust its working regime to the frequency content of the thalamus inputs.

When the system is nonlinear, theory predicts that resonances appear at every rational ratio  $k/l$  of  $\omega_H/\omega_F$ , although in real oscillatory systems, the maximum and width of the resonance decrease with  $|k| + |l|$ : resonances occur only for frequency ratios  $1/2$ ,  $1$ , and  $2$ . The perturbation parameter  $\delta\omega \stackrel{def}{=} \omega_H - \frac{k}{l}\omega_F$  is a fundamental parameter for the description of the  $k:l$  resonance peak. Compared to linear resonance, many more new network responses can be produced. For subharmonic forcing  $\omega_F < \omega_H$ , the PL frequency is the same as the forcing frequency. For superharmonic forcing  $\omega_H > \omega_F$ , the periodic responses frequencies are a fraction of the forcing frequency  $\frac{\omega_F}{l}$ , thereby producing again a phase-locked (to the input) solution. Hence, we will also call them PL. In addition, there can be multistability of PL and modulated responses with two intrinsic frequencies that we call torus solutions or quasiperiodic solutions. The resonance curve is then the amplitude of the response (PL/torus) as a function of the forcing frequency  $\omega_F$ .

In earlier work along these lines (Pollina, Benardete, & Noonburg, 2003; Ledoux & Brunel, 2011; Decker & Noonburg, 2012), the multistability of PL solutions was studied around the 1:1 peak. One can find a resonance curve in the periodic forcing of spatially extended ISN networks in Rule, Stoffregen, and Ermentrout (2011). Resonance effects in neural masses have also been studied in Spiegler, Knösche, Schwab, Haueisen, & Atay (2011), though without addressing dynamics. There are general limitations to the phase reset curve (PRC) as a description of neural oscillators; in particular, the size of the perturbation has to be small. For example in Wedgwood, Lin, Thul, and Coombes (2013), Morris-Lecar neurons forced by very brief periodic kicks produce chaotic responses that are captured by an adequate phase-amplitude description but not by a phase description alone.

Understanding the properties of the resonances of an oscillatory system is extremely difficult in general. Here, by looking at the ISN, which we show are tuned close to a Hopf bifurcation, we are able to understand thoroughly the possible network responses PL/torus. The periodic forcing of a Hopf bifurcation has been studied in Gambaudo (1985) for the responses near all strong resonances. However, the link to our model is buried in multiple changes of variables. Recently, the resonance curves were classified in Zhang and Golubitsky (2011) around the 1:1 resonance. One issue is that

the authors focused solely on PL solutions and hence the torus solutions were not considered and the resonances curves are incomplete. A second issue is that they did not examine the stability of the PL responses, which limits the predictive power of the analysis. Here, we compute the changes of variables that provide the normal form as in Gambaudo (1985), and we also provide several formulas concerning the resonance curves. This is technical and lengthy but not too difficult (see the appendixes). This allows us to achieve a complete understanding of the resonance curves, which allowed us to recover some previous results (Zhang & Golubitsky, 2011).

Finally, we introduce a type of network similar to the ISN but that supports sustained oscillations (SO), for example, those that are induced by carbachol. The E-I network that we then consider can be tuned to either the ISN or the SO regime.

The plan of the study is as follows. After presenting the model and the general method, which is mainly the use of bifurcation theory, we study in detail the main resonances 1:1, 1:2, 2:1 of an unforced E-I network in the ISN regime. In the discussion, we put these results into an experimental context.

## 2 Description of the Model and Definitions

---

We analyze a rate model with two populations of excitatory and inhibitory neurons (E-I network). More specifically, we consider a Wilson-Cowan model describing the firing rate of each population:

$$\begin{cases} \tau_E \dot{E} = -E + S(J_{EE}E + J_{EI}I + \theta_E(t)), \\ \tau_I \dot{I} = -I + S(J_{IE}E + J_{II}I + \theta_I(t)), \end{cases} \tag{2.1}$$

where  $S$  is the sigmoid function:

$$S(x) = \frac{1}{1 + e^{-x}}.$$

The variables  $\theta_E, \theta_I$  describe the total presynaptic current onto each population, and  $\tau_E, \tau_I$  are the time constants of each population. Finally, the connections are such that  $J_{EE}, J_{IE} > 0$ , and  $J_{EI}, J_{II} < 0$ . The total presynaptic currents ( $\theta_E(t), \theta_I(t)$ ) are supposed to be periodic functions of time with only one Fourier component:

$$\begin{bmatrix} \theta_E(t) \\ \theta_I(t) \end{bmatrix} = \begin{bmatrix} \theta_E^{(0)} \\ \theta_I^{(0)} \end{bmatrix} + \epsilon \cos(\omega_F t) \begin{bmatrix} \theta_E^{(1)} \\ \theta_I^{(1)} \end{bmatrix}, \tag{2.2}$$

where  $\epsilon \ll 1$  is the (small) forcing amplitude and  $\frac{\omega_F}{2\pi}$  is the forcing frequency. An important quantity is the perturbation. For a rational approximation of the ratio  $\frac{\omega_H}{\omega_F} \approx \frac{k}{l}$  where  $\frac{\omega_H}{2\pi}$  is the gamma frequency of the rhythms generated by the E-I network, the perturbation is defined by

$$\delta\omega \stackrel{def}{=} \omega_H - \frac{k}{l}\omega_F.$$

A phase-locked (PL) solution is a time-periodic network response of equation 2.1 with frequency  $\omega_F/l/2\pi$ ,  $l > 0$  integer, fraction of the forcing frequency. A quasiperiodic network response  $V(t)$ , or torus solution, is a response with two frequency components  $V(t) = f(\omega_1 t, \omega_2 t)$  where  $f$  is  $2\pi$ -periodic in each variable (see, for example, Figure 9, top).

### 3 Methods

---

This section introduces the parts of dynamical systems and bifurcation theory needed to understand the behaviors of network 2.1 when the forcing frequency  $\omega_F$  and the forcing amplitude  $\epsilon$  are varied. The equations can be rewritten as  $\dot{V} = F(V, t, \mu)$  where  $V = (E, I)$  and  $\mu$  is the vector of parameters. When  $\epsilon = 0$ , the system is autonomous and  $F(V, t, \mu) \stackrel{\epsilon=0}{=} F^0(V, \mu)$ . We first choose  $\mu$  so that the unforced network  $\dot{V} = F^0(V, \mu)$  is in an ISN regime and study the effect of forcing terms. In particular, we focus on the amplitudes of the time-periodic and quasiperiodic solutions of equation 2.1.

Recall that an equilibrium state is a point  $V^f$  where the vector field  $F^0(\cdot, \mu)$  vanishes. A bifurcation occurs when there is a qualitative change in behavior or stability as the parameters  $\mu$  are varied (for a more precise definition, see Guckenheimer & Holmes, 1983, and Kuznetsov, 2004). Bifurcations can be detected by looking at the stability of the equilibrium, which is stable if the eigenvalues of the Jacobian of  $F^0$  at  $(V^f, \mu)$  have negative real parts. When  $\mu$  is varied, the eigenvalues move in the complex plane, and when two complex conjugate eigenvalues cross the imaginary axis without vanishing for  $\mu = \mu_H$ , the system undergoes what is called a Hopf bifurcation signaling the appearance or disappearance of periodic solutions (modulo some nondegeneracy conditions). The set of bifurcation points partitions the parameter space in sets of similar local dynamics, called a bifurcation diagram. Close to a bifurcation point, the vector field  $F^0$  can be simplified by a change of variables into its normal form, which is the polynomial approximation with the fewest monomials.

The analysis of the forced system proceeds by writing the activity as  $V = V^f + 2\Re(z(t)e^{i\omega_F \frac{k}{l} t} \zeta) + \text{higher-order terms (h.o.t.)}$ , that is, monomials  $z^p \bar{z}^q e^{i\omega_F t(n + \frac{k}{l}(p-q))}$ ,  $p + q > 1$ . This expression is then substituted into  $\dot{V} = F(V, t, \mu)$  to obtain a normal form,  $\dot{z} = \alpha z + \beta z|z|^2 + \dots$ , which may depend on time. Note that when  $z = 0$ , the network response is an equilibrium,

whereas when  $z(t) = z_0$ , the network response is periodic in time. Finally, a periodic solution  $z(t)$  corresponds to a torus response of the network. Analysis of the differential equation in  $z$  with bifurcation theory allows us to predict the network responses and resonances.

**3.1 ISNs Are Close to a Supercritical Hopf Bifurcation.** The parameters of the model are chosen for the ISN regime, which exhibits damped oscillations in the gamma range. An ISN satisfies the following properties (Tsodyks et al., 1997):

1. When the interpopulation connections  $J_{IE} = J_{EI} = 0$  are zero, an equilibrium and, more precisely, a (stationary) excitatory firing rate  $E^f$  solution of  $E^f = S(J_{EE}E^f + \theta_E)$ , is unstable:  $-1 + J_{EE}S'(J_{EE}E^f + \theta_E) > 0$ .
2. When the interpopulations connections are reestablished, there is a stable equilibrium  $(E^f, I^f)$  solution of  $(\dot{E} = \dot{I} = 0)$  that is stable: all the eigenvalues of the Jacobian at  $(E^f, I^f)$  have negative real parts.

Assume that this is the same equilibrium, at some point between these two extremes, the eigenvalues  $\pm i\omega_H$  of the Jacobian at the equilibrium have zero real parts with nonzero imaginary parts and the network undergoes a Hopf bifurcation signaling the appearance or disappearance of  $\frac{2\pi}{\omega_H}$ -periodic solutions. (see Kuznetsov, 2004). Note that for an ISN,  $J_{EE}$  is relatively small at point 1 above.

**Remark 1.** The fact that the eigenvalues of the Jacobian are complex and not real (hence zero) at the instability is not a restriction. Almost any perturbation of a network with real eigenvalues yields complex eigenvalues.

The Hopf bifurcations can then be found by varying the inputs  $\theta_E$  and  $\theta_I$  in equation 2.1 (Wilson & Cowan, 1972; Borisyuk & Kirillov, 1992; Hoppensteadt & Izhikevich, 1997). The Hopf bifurcation curves (red) in the plane  $(\theta_E^{(0)}, \theta_I^{(0)})$  are shown in Figure 2. The red-shaded region in the left panel corresponds to the parameters where the E-I network produces sustained oscillations (SO) and the gray-shaded region corresponds to the ISN working regime with damped oscillations.

Close to the Hopf curves (red), there is a good polynomial approximation of equation 2.1, called the Hopf normal form, whose coefficients are important in determining how the E-I network responds to constant inputs  $\theta_E^{(0)}, \theta_I^{(0)}$ . We will consider the case of the inhibitory current  $\theta_I^{(0)}$  as a parameter. More precisely, if  $\zeta$  is the eigenvector of the Jacobian for the eigenvalue  $i\omega_H$  and

$$(E, I) = (E^f, I^f) + z\zeta + \bar{z}\bar{\zeta} + \Psi(z, \bar{z}), \tag{3.1}$$

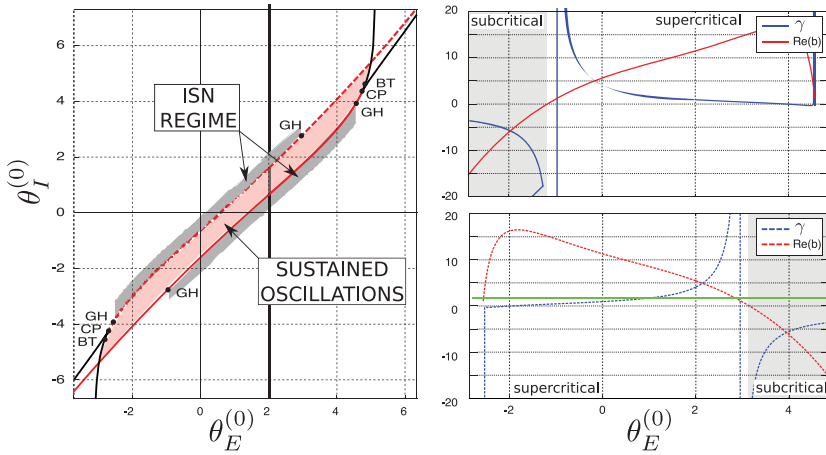


Figure 2: Bifurcation diagram of the E-I network. (Left) Hopf bifurcation curves (red) and Fold bifurcation curves (black) in the plane  $(\theta_E^{(0)}, \theta_I^{(0)})$ , generalized Hopf bifurcation point (GH), Bogdanov-Takens bifurcation point (BT), cusp bifurcation point (CP). (Right) Hopf normal form coefficient  $\Re(b)$  (red) and shear  $\gamma$  (blue). The green curve equation is  $\gamma = \sqrt{3}$ . Dashed and continuous curves correspond to the dashed and continuous Hopf curve, respectively, in the left panel. The ISN regions have a gray background. Parameters:  $J_{EE} = 10$ ,  $J_{EI} = -12$ ,  $J_{IE} = 10$ ,  $J_{II} = -10$ , and  $\tau_E/\tau_I = 3/8$ . (Diagrams computed with the MatCont.)

where  $\Psi$  is a higher-order polynomial, then

$$\dot{z} = z(\omega_H + a\delta\theta_I^{(0)} - b|z|^2) + h.o.t., \tag{3.2}$$

where  $\delta\theta_I^{(0)} \stackrel{def}{=} \theta_I^{(0)} - \theta_{I,Hopf}^{(0)}$  and the *h.o.t.* of the polynomial in  $z$  are negligible. To completely characterize the behavior of the network, we need to compute the complex coefficients  $a, b$  as a function of the network parameters. Recall that the Hopf bifurcation is said to be supercritical when  $\Re b > 0$  and subcritical when  $\Re b < 0$ . Computing the Lyapunov coefficient  $b$  and the linear coefficient  $a$  is difficult even when an analytical expression exists (see, e.g., Guckenheimer & Holmes, 1983; Kuznetsov, 2004). Hence, we compute them here numerically. In the right panel of Figure 2, we plot for each Hopf curve (dashed and continuous) the real part of  $b$  and the shear  $\gamma$  defined by

$$\gamma \stackrel{def}{=} \frac{\Im(b)}{\Re(b)}. \tag{3.3}$$

Table 1: Link between the E-I Network Working Regime with the Internal Parameters.

Regime	Condition
ISN	$\Re(a)\delta\theta_I^{(0)} < 0$
SO	$\Re(a)\delta\theta_I^{(0)} > 0$

When equation 3.2 is expressed in polar coordinates, it is apparent that the shear acts on the phase variable, speeding up or slowing the phase as a function of the radius. Hence, it describes how the flow is distorted along the phase variable. Note that the shear becomes infinitely large when the network is close to the generalized Hopf points or the Bogdanov-Takens points in the right panel of Figure 2.

For the network response to an inhibitory transient input to produce damped oscillations (Tsodyks et al., 1997), the working regime of the ISN should be close to a supercritical Hopf bifurcation. In contrast, close to a subcritical Hopf bifurcation with a bounded nonlinearity  $S(x)$ , the bifurcation diagram of equation 2.1 resembles that of a class II neuron, which exhibits an undesirable bistability between large-amplitude oscillations and the constant solution rather than a damped oscillation in response to a transient inhibitory input.

**Definition 1.** *We therefore assume that the ISN regime of a two-population network is close to a supercritical Hopf bifurcation where  $\Re b > 0$ .*

The consequences of  $\Re b > 0$  are most easily seen in polar coordinates for  $z$ . For  $\Re a\delta\theta_I^{(0)} > 0$ , the stable response is given by  $z(t) = \sqrt{\frac{\Re(a\delta\theta_I^{(0)})}{\Re b}} e^{i\omega t + \phi}$ ,  $\omega \approx \omega_H$ , which are network sustained oscillations. For the other case, the stable response is  $z(t) = 0$ . Thus, the term  $\Re(a)\delta\theta_I^{(0)}$  controls which regime the network is in, as summarized in Table 1.

Rephrasing these mathematical results, to be in an ISN regime an E-I network needs to be close to a Hopf bifurcation, effectively acting as a Stuart-Landau oscillator as described by the normal form in equation 3.2. The parameter  $\Re(a)\delta\theta_I^{(0)}$  controls whether the network is in an ISN or SO regime.

An example of the phase plane and nullclines for the unforced model in the two regimes ISN and SO is shown in Figure 3.

**3.2 Numerical Study of the Phase-Locked Responses.** We study the effect of driving the network described in the previous section with periodic inputs with forcing frequency  $\frac{\omega_F}{2\pi}$  (see equation 2.1).

**Definition 2.** *A  $k:l$  resonance occurs when  $\omega_F$  is a rational fraction of  $\omega_H$ :  $\frac{\omega_F}{\omega_H} = \frac{l}{k}$ .*

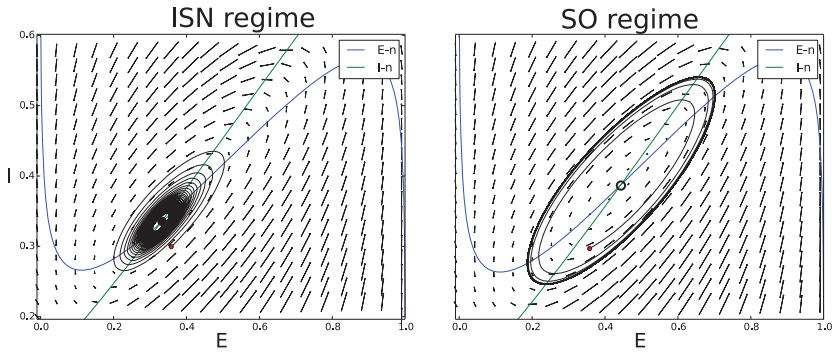


Figure 3: Phase-plane examples of the dynamics. Plot of the nullclines  $\dot{E} = 0$  (blue) and  $\dot{I} = 0$  (green) in the ISN regime (left plot,  $\theta_E^{(0)} = 0$  and  $\theta_I^{(0)} = -0.647$ ) and in the SO regime (right plot,  $\theta_E^{(0)} = 0$  and  $\theta_I^{(0)} = -1$ ). Examples of two trajectories are shown in black with initial conditions indicated with a red dot. In the ISN regime, the convergence of the trajectory to the stable equilibrium is not shown completely for illustration reasons. In the SO regime, the trajectory converges to a limit cycle.

For a given forcing amplitude, we computed numerically (using software Auto07p) the PL responses as function of the forcing frequency as shown in Figure 4. The stable responses are shown in black and the unstable ones in dashed gray.

In linear systems, periodic forcing close to the intrinsic frequency  $\frac{\omega_H}{2\pi}$  leads to a large increase in the amplitude of the response characterized by a bell-shaped curve in the amplitude of the response versus forcing frequency called a resonance curve. This is seen in Figure 4 for  $\omega_F \approx \omega_H$ .

Because the ISN is poised close to a Hopf bifurcation, several new phenomena arise. There are three additional peaks at ratios 3:1, 2:1, and 1:2 and multistability (right panel of Figure 4), as previously reported (Decker & Noonburg, 2012; Pollina et al., 2003).

Note that the analysis of the PL solutions fails to predict the network response for  $\omega_F \approx 1.5 \omega_H$  in the right panel of Figure 4 because the PL solutions are unstable. The stable network response is a torus solution.

When forced at frequency  $2\omega_H/2\pi$ , the stable response of the network is a PL solution with frequency  $\frac{\omega_H}{2\pi}$ ; that is, there is period doubling in the response of the network. There are additional phenomena near  $\omega_F \approx 2 \omega_H$  that will be explained more precisely in the following sections.

**3.3 Theoretical Properties of the Network Resonances.** In this section, we study the nonlinear resonance curves using the normal form approximation. Periodic forcing of a Hopf bifurcation has been systematically studied (Arnold, 1988; Gambaudo, 1985; Zhang & Golubitsky, 2011). The

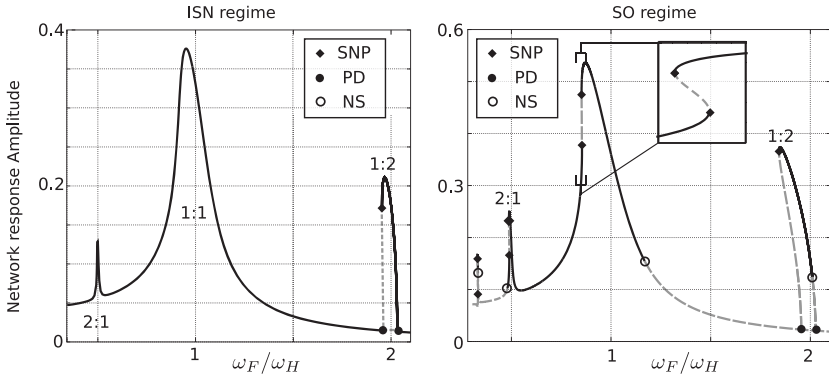


Figure 4: Amplitude of the phase-locked solutions as a function of the forcing frequency. (Left) Plot of the amplitude of the PL solutions for the same network as in Figure 2 in the ISN regime; parameters are  $\epsilon = 0.07$ ,  $\theta_E^{(0)} = 0$ , and  $\theta_I^{(0)} = -0.647$  ( $\theta_{I,Hopf}^{(0)} = -0.647759$ ). (Right) Amplitude plot for parameters of the forcing current in the SO regime:  $\epsilon = 0.11$ ,  $\theta_E^{(0)} = 2$ , and  $\theta_I^{(0)} = 1.5874$  ( $\theta_{I,Hopf}^{(0)} = 1.595384$ ). Black lines are stable; dashed gray lines are unstable. SNP: saddle node of periodic solution. NS: Neimark-Sacker bifurcation. PD: period doubling bifurcation.

dynamics of the forced network response amplitude close to the  $k:l$  resonance is (Elphick, Iooss, & Tirapegui, 1987):

$$\dot{z} = z(a\delta\theta_I^{(0)} + c_1 + i\delta\omega - b|z|^2) + c_2\bar{z}^{l-1} + h.o.t., \tag{3.4}$$

where  $\delta\omega = \omega_H - \frac{k}{l}\omega_F$  is the perturbation parameter and

$$\begin{cases} (E(t), I(t)) = (E^f, I^f) + z(t)e^{i\frac{\omega_F k}{\omega_F} t} \zeta + \bar{z}(t)e^{-i\frac{\omega_F k}{\omega_F} t} \bar{\zeta} + \Psi(z(t)e^{i\frac{\omega_F k}{\omega_F} t}, \\ \bar{z}(t)e^{-i\frac{\omega_F k}{\omega_F} t}, \mu, t), \\ \mu \stackrel{def}{=} (\delta\theta_I^{(0)}, \epsilon, \omega), \end{cases} \tag{3.5}$$

where  $t \rightarrow \Psi(\cdot, \cdot, \cdot, t)$  is  $\frac{2\pi}{\omega_F}$ -periodic (see appendix A) and represents polynomials of order at least 2 whose contribution can be neglected because  $|z| \ll 1$ . Note that the coefficients  $c_1, c_2$  have to be computed as functions of the network parameters  $\epsilon, \delta\omega$  (see the appendixes) while the other coefficients are the same as in equation 3.2. The normal form, equation 3.4, describes the network response amplitude  $z$  as a dynamical object.

We will focus on the resonances 1:1, 1:2, and 2:1 for which  $l = 1, 2$  and use the perturbation parameter  $\delta\omega$  as a small parameter. By definition,

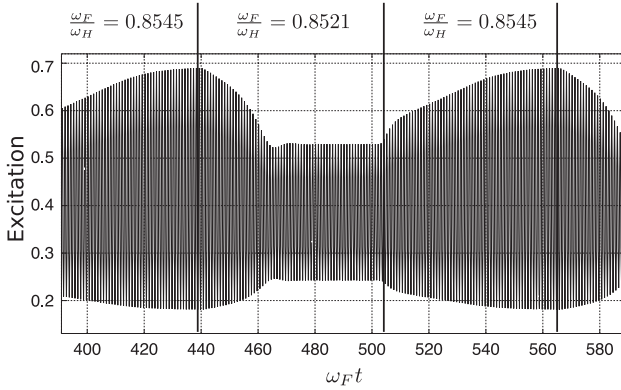


Figure 5: Example of a multistable response. Plot of the excitatory population response amplitude for  $\omega_F$  close to  $0.853 \omega_H$ . Note that  $\omega_F$  is slowly modulated to show the change between the stable states in the multistability region of Figure 4 (right). The figure shows a jump between two PL solutions of different amplitudes.

around each resonance peak, the resonance curve is approximated by the function  $\delta\omega \rightarrow |z|$  where  $z$  is solution of  $\dot{z} = 0$  in equation 3.4.

The resonance curve near the resonance 1:1 was partially characterized in Zhang and Golubitsky (2011) and can be quite complicated. In the ISN regime only two types of resonance curves are possible (see Figure 11). However, Zhang and Golubitsky (2011) did not examine the stability of the PL solution. We propose to fill the gap in the following analysis. Here are some important properties of the main resonances that we prove in the following sections:

1. The maximum of the 1:1 peak is not centered on  $\omega_H$  when  $\Im(b) \neq 0$ .
2. There is multistability (and hysteresis near the peaks 1:1, 2:1) in the ISN regime if and only if the shear  $\gamma$  (see equation 3.3) satisfies  $|\gamma| > \sqrt{3}$ . See section 3.4 and also Zhang and Golubitsky (2011) for a proof. An example of hysteresis is shown in Figure 5. If the forcing amplitude  $\epsilon$  is too small, the multistable PL disappear.
3. If the forcing amplitude  $\epsilon$  is large enough, the maximum  $M$  of the 1:1 resonance peak satisfies  $\epsilon^{1/3}/2^{1/6} < M \frac{|\Re b|^{1/3}}{|\tilde{c}_2|} < \epsilon^{1/3}$  where  $c_2 \stackrel{def}{=} \epsilon \cdot \tilde{c}_2$  (see Golubitsky, Shiau, Postlethwaite, & Zhang, 2009). As  $\epsilon \ll 1$ , it gives a very large amplification of the corresponding forcing frequency component. We plot the maximum of the resonance peaks 1:1, 1:2, 2:1 in log-log coordinates in Figure 6.
4. No torus responses are possible in the ISN regime near the 1:1 and 1:2 resonances.

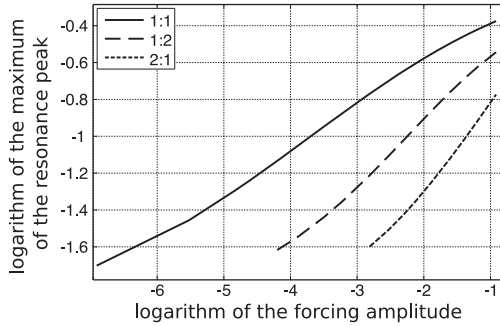


Figure 6: Power law for the maximum of the resonance peaks. Log of the resonance peak power for 1:1, 1:2, 2:1 as a function of the log of the forcing amplitude  $\epsilon$ . Network parameters as in Figure 4, right.

Given these properties, it is straightforward to select a network that shows one of these features. For example, to have multistability, we need a large enough shear (see Figure 2, right, and Figure 4, right). For torus solutions, the network should be in the SO regime.

**3.4 Case of 1:1 Resonance.** How do the different PL solutions interact? Can the torus solution exist together with multistable PL solutions? Are there any other behaviors? We explore these questions for the 1:1 resonance. The coefficients of the general normal form, equation 3.4, around the resonance 1:1 are given in appendix A:

$$\dot{z} = z(a\delta\theta_I^{(0)} + 1(\omega_H - \omega_F) - b|z|^2) + \frac{\epsilon}{2}\langle DS \theta^{(1)}, \zeta^* \rangle, \tag{3.6}$$

where  $DS \theta^{(1)} \stackrel{def}{=} (\theta_E^{(1)} S'(J_{EE} E^f + J_{EI} I^f + \theta_E^{(0)}), \theta_I^{(1)} S'(J_{IE} E^f + J_{II} I^f + \theta_I^{(0)}))$ . Recall that from definition 3.5 of  $z$ , the PLL solutions are equilibria solving

$$0 = z(a\delta\theta_I^{(0)} + 1(\omega_H - \omega_F) - b|z|^2) + \frac{\epsilon}{2}\langle DS \theta^{(1)}, \zeta^* \rangle.$$

All possible responses of the forced network near the resonance 1:1 can be obtained by studying the dynamics generated by equation 3.6 as a function of the parameters  $\omega_F, \epsilon, \theta^{(0)}$ . There are at least three parameters— $\delta\theta^{(0)}, \epsilon$ , and  $\delta\omega$ —which makes the analysis difficult. However, equation 3.6 can be further simplified using appropriate scaling  $t = \alpha t', z = \beta Y$  (see appendix D), to an equation with two parameters:

$$\dot{Y} = Y(\epsilon_0 + 1\tau - |Y|^2)e^{i \arg b} + \rho, \tag{3.7}$$

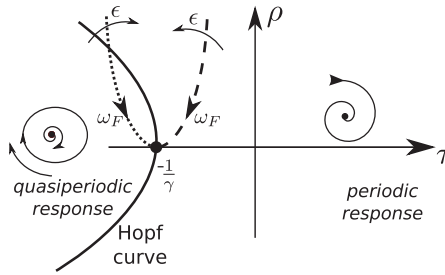


Figure 7: Dynamics for the amplitude of the network response in the case  $\epsilon_0 = -1$ . Bifurcation diagram of equation 3.6 in the plane  $(\tau, \rho)$ . The dashed curves are the resonance curves parameterized by the perturbation  $\delta\omega$  (dashed for the ISN regime, dotted for the SO regime). Adapted from Gambaudo (1985).

where  $Y \in \mathbb{C}, \rho \geq 0, \tau \in \mathbb{R} \rho > 0$  and

$$\begin{cases} \epsilon_0 = \text{sign}(\delta\theta_l^{(0)}(\Re a + \gamma \Im a) + \gamma \delta\omega) = \pm 1 \\ \rho^{2/3} = \frac{\Im(b)}{\Re(a)\delta\theta_l^{(0)}} \left(\frac{|c_2|}{|b|}\right)^{2/3} \left(\frac{\epsilon_0}{\gamma} - \tau\right), \quad c_2 \stackrel{\text{def}}{=} \frac{\epsilon}{2} \langle DS \theta^{(1)}, \zeta^* \rangle \end{cases} \quad (3.8)$$

(see appendixes D and E). The complete bifurcation diagram of equation 3.7 can be found in Arnold (1988) and Gambaudo (1985). The case  $\epsilon_0 = -1$ , shown in Figure 7, is a torus solution ( $Y$  is time-periodic) when  $\tau$  is sufficiently negative. The case  $\epsilon_0 = 1, \gamma > 1/\sqrt{3}$  is shown in Figure 8, and the case  $\epsilon_0 = 1, 0 < \gamma < 1/\sqrt{3}$  can be found in Gambaudo (1985).

**3.5 Description of the Phase Diagram in the Case  $\epsilon_0 = 1$ .** The equilibria of the phase diagrams in Figure 8 are marked with red dots and represent PL network responses. Time-periodic solutions correspond to the quasiperiodic network responses, such as the top one in Figure 9. Two curves are particularly interesting in Figure 8: the curve of saddle-node bifurcations (blue), which signals the appearance or disappearance of equilibria (marked as red dots), and the Hopf bifurcation curve (red), which signals the appearance or disappearance of periodic orbits. The saddle-node curves give the parameter regions corresponding to multistable PL, such as phase diagram numbers 3 and 11 in Figure 8.

Hence, between the phase diagrams 3 and 4, a torus response is created by a Hopf bifurcation. The period of the response amplitude increases without bound as the parameters go from the phase diagram 4 to 5 (or 11 to

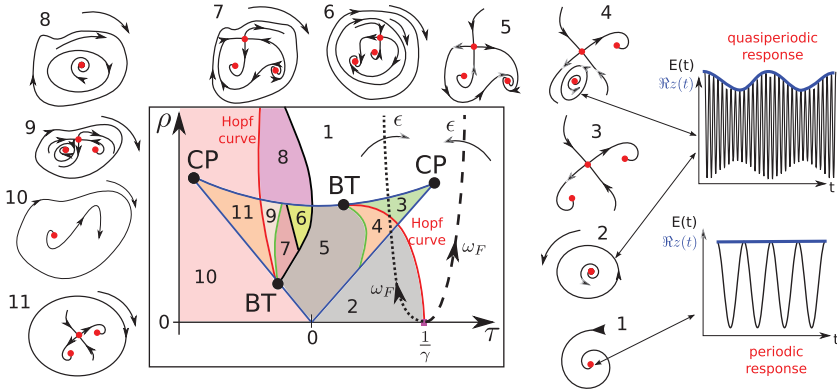


Figure 8: Dynamics for the amplitude of the network response in the case  $\epsilon_0 = 1, \gamma > 1/\sqrt{3}$ . Bifurcation diagram of equation 3.6 in the plane  $(\tau, \rho)$ . Red: curve of Hopf bifurcations. Blue: curve of saddle-node bifurcations. BT: Bogdanov-Takens bifurcation point. The dashed curves in black are the resonance curves parameterized by the perturbation  $\delta\omega$  (dashed for the ISN regime, dotted for the SO regime). The CP points have coordinates  $(\pm\frac{1}{\sqrt{3}}, \frac{2\sqrt{2}}{3\sqrt{3}})$ . The BT points have abscissa  $\pm\frac{mb}{3b+2}$ . Adapted from Gambaudo (1985). On the right, we show the link between the dynamics of the amplitude  $z(t)$  (or  $Y(t)$ ) and  $E(t)$ .

9) to the homoclinic bifurcation curve. An example of such a phenomenon of a homoclinic response is shown in Figure 9.

**Remark 2.** Some effects are not captured by the normal form analysis. Along the Hopf curves, the frequency  $\omega_{amp}$  of the response amplitude tends to zero at the BT points and the frequency  $\omega_{amp}$  can be such that  $\frac{\omega_{amp}}{\omega_H}$  is rational, leading to Arnold tongues and possibly strong resonances. The same resonances can occur when going from the Hopf curves to the homoclinic curves. Hence, in phase diagrams 4 and 9 in Figure 8, there is a “torus breakdown” (see Kuznetsov, 2004), usually associated with chaotic behavior of equation 2.1 in which the torus solution becomes highly irregular.

*3.5.1 Application to the Study of the Response.* We now study the specific effects of the three parameters  $\epsilon, \omega_F, \delta\theta^{(0)}$  on the response of the forced network. In appendix E, we show that the three parameters describe a curve given by the second equation in 3.8 in the plane  $(\tau, \rho)$  which is parameterized by the perturbation parameter  $\delta\omega$ . They are plotted in Figures 7 and 8 using dashed curves of equation. Recall that the resonance curve is given by  $RC: \delta\omega \rightarrow |z|$  where  $z$  is the solution of  $\dot{z} = 0$  in equation 3.6. It can be solved by taking some norm in equation 3.6. Using the equivalent equation, 3.7, one sees that  $RC(-\delta) = RC(\delta)$  if the shear is zero:  $\gamma = 0$ . Computing

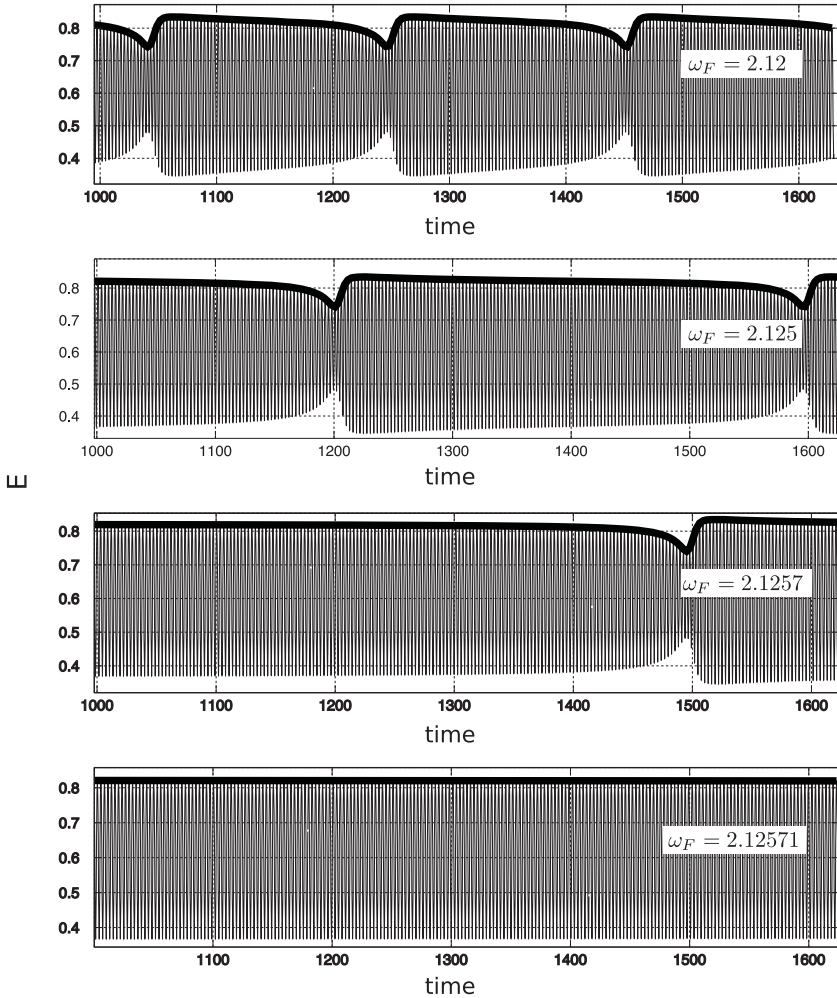


Figure 9: Example of convergence to a homoclinic response. Plot of the excitatory response for different forcing frequencies. The forcing parameters are such that the dynamics is close to the homoclinic curve. Different parameters from Figure 4, right, are  $\theta_i^{(0)} = 0.824174$ ,  $\epsilon = 0.05$ .

the resonance curve amounts to computing the equilibria as a function of the perturbation. But we can also predict the dynamics corresponding to a particular value of the perturbation. Indeed, when the perturbation is varied, the couple  $(\tau, \rho)$  describes a curve of the second equation in 3.8 in the bifurcation diagram that allows predicting the response of the forced network.

The two types of curves, depending on the network regime (ISN or SO), are shown in Figures 7 and 8. When the forcing frequency or the perturbation is varied, the value of  $\epsilon_0 \stackrel{def}{=} \text{sign}(\delta\theta^{(0)}(\Re a + \gamma \Im a) + \gamma(\omega_H - \omega_F))$  changes, which has the consequence of switching the possible response dynamics between Figures 7 and 8.

More precisely, if  $\omega_F > \omega_H + \frac{\delta\theta^{(0)}}{\gamma}(\Re a + \gamma \Im a)$ , the possible dynamics correspond to the one of Figure 7 whereas if  $\omega_F < \omega_H + \frac{\delta\theta^{(0)}}{\gamma}(\Re a + \gamma \Im a)$ , then the possible dynamics correspond to the one of Figure 8.

We next examine the working regimes for ISN and SO in more detail.

**3.5.2 The ISN Regime.** Recall that this case corresponds to  $\Re(a\delta\theta^{(0)}) < 0$  which forces  $\frac{\epsilon_0}{\gamma} \leq \tau$  from the second equation in 3.8. When Figures 7 and 8 are used, the resonance curve never crosses the Hopf bifurcation curve, and the network cannot produce torus solutions (see appendix C). Also, if  $\Re(a\delta\theta^{(0)}) \approx 0$ , the resonance curve (dashed black) is almost vertical and intersects the Saddle-node bifurcation curve iff  $\frac{1}{\gamma} < \tau_{CP} = \frac{1}{\sqrt{3}}$ , that is,  $\gamma > \sqrt{3}$ , the condition given in Zhang and Golubitsky (2011) ensuring multistability. Indeed, in this case, the resonance curve crosses the region labeled 3 in Figure 8, where two stable equilibria are present. The same occurs when the shear  $|\gamma|$  is increased. In the right panel of Figure 4,  $|\gamma| > \sqrt{3}$  using the numerical values of the shear given in Figure 2. Finally, if the forcing amplitude  $\epsilon$  increases, the regime of multistable PL becomes larger (if  $|\gamma| > \sqrt{3}$ ) because the curve will shift from phase diagram 1 to phase diagram 3 (see the effect of the forcing amplitude  $\epsilon$  on the curve in Figure 8). As a consequence, the only possible dynamics in the ISN regime are the ones labeled 1 and 3 in Figure 8.

Thus, the forced ISN network can only produce periodic responses and multistable periodic responses that we call PL solutions.

**3.5.3 The SO Regime.** The SO regime gives rise to a richer behavior than the ISN regime because  $\frac{\epsilon_0}{\gamma} \geq \tau$  from the second equation in 3.8. In particular, the resonance curve can cross the Hopf curve, which generates torus solutions such as those in regions 2 and 4 in Figure 8. Reducing the forcing amplitude  $\epsilon$  yields more dynamical effects as the resonance curve passes through all parts of the phase diagrams in Figure 8. It is, for example, straightforward to select an amplitude  $\epsilon$  that produces an almost homoclinic response (green curve in Figure 8) as in Figure 9, or multistability between PL and torus responses (e.g., phase diagram 6 of Figure 8), or large-amplitude torus responses as in phase diagrams 10 and 11. In contrast to the ISN regime, increasing the forcing amplitude leads to simpler dynamics.

Therefore, the SO regime can produce periodic responses, quasiperiodic responses, or even stranger behaviors like the one in Figure 9. Hence, the

resonance curve is not enough to describe the dynamics (see the incomplete case in Figure 4, right, and one needs to at least compute and plot the quasiperiodic responses. This is done numerically in the section 3.8.

**3.6 Case of the 2:1 Resonance.** The shape of the resonances for the cases 1:1 and 2:1 are qualitatively similar (see equation 3.4) because  $l = 1$  in both cases. In particular, a necessary and sufficient condition for the 2:1 resonance curve to display multistability is (see the study of the 1:1 resonance)

$$|\gamma| > \sqrt{3}. \tag{3.9}$$

The dynamics are the same as in Figures 7 and 8, albeit occurring in a much narrower parameter region.

**3.7 Case of the 1:2 Resonance.** This case is different from the 1:1 and 2:1 resonances. Let us write the network response  $(E(t), I(t))$  around the basal activity  $(E^f, I^f)$  as

$$\begin{cases} (E(t), I(t)) = (E^f, I^f) + z(t)e^{i\frac{\omega_F}{2}t}\zeta + \bar{z}(t)e^{-i\frac{\omega_F}{2}t}\bar{\zeta} + \Psi(z(t)e^{i\frac{\omega_F}{2}t}, \\ \bar{z}(t)e^{-i\frac{\omega_F}{2}t}, \mu, t), \\ \mu \stackrel{def}{=} (\delta\theta_I^{(0)}, \epsilon, \omega), \end{cases} \tag{3.10}$$

where  $t \rightarrow \Psi(\cdot, \cdot, \cdot, t)$  is  $\frac{2\pi}{\omega_F}$ -periodic (see appendix A for an explanation) and represents a polynomial of order at least 2 whose contribution is negligible because  $|z| \ll 1$ . The dynamics of the amplitude around the 1:2 peak is governed by

$$\dot{z} = z(a\delta\theta_I^{(0)} + 1(\omega_H - \omega_F/2) - b|z|^2) + c_2\bar{z}, \tag{3.11}$$

where  $c_2$  is proportional to the forcing amplitude  $\epsilon$  (see the appendix B). Unlike the previous cases,  $z = 0$  is the solution of this equation corresponding to the network response  $(E(t), I(t)) = (E^f, I^f) + \Psi(0, 0, \mu, t)$ ; the response frequency is  $\frac{\omega_F}{2\pi}$ . On the other hand, the nontrivial constant solutions in  $z$  correspond to PL responses at frequency  $\frac{\omega_F}{4\pi}$ , that is, half the forcing frequency from equation 3.10. Thus, the PL solution undergoes a period-doubling bifurcation around  $\omega_F \approx 2\omega_H$  (see Figure 4).

The shape of the 1:2 resonance peak can be found by solving  $\dot{z} = 0$  in the previous equation, which leads to a quadratic equation in  $|z|^3$  (see appendix F). It always has the qualitative shape shown in Figure 4. In appendixes F and G, we prove the following properties concerning the 1:2 peak:

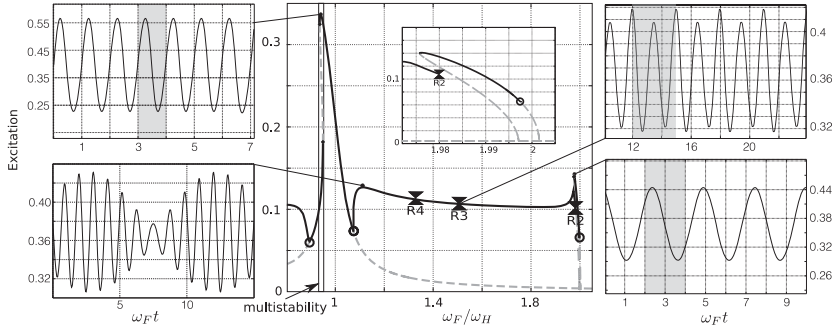


Figure 10: Example of resonance curve in the SO regime. Plot of the amplitude of the response as function of forcing frequency. The gray box shows one period of a periodic response. See the text for further explanation. Parameters:  $\epsilon = 0.01$ ,  $\delta\theta^{(0)} = -0.0018$ . Same network as in Figure 2. The torus solution is continued until the resonance R2 where the continuation fails. (Computed with Auto07p and Knut.)

1. The 1:2 resonance peak exists only if the forcing amplitude is large enough:  $|c_2| > |\Re\delta\theta_1^{(0)}|$ .
2. The width  $W$  of the peak scales linearly with the forcing amplitude  $W \sim \epsilon$ .
3. The height  $H$  of the peak scales linearly with the forcing amplitude  $H \sim \epsilon$ .
4. In the ISN regime, quasiperiodic network responses are not possible.

We do not show all the possible responses for the 1:1 peak due to a lack of space. However, all of the responses in the ISN regime are listed in appendix G. In other words, the 1:2 case has the remarkable feature that when the ISN is forced at frequency  $\approx \frac{2\omega_H}{2\pi}$ , it has a periodic response with frequency  $\frac{\omega_H}{2\pi}$ . This could explain why this peak was not seen in Cardin et al. (2009), for example.

**3.8 Completion of the Resonance Curves in the SO Regime.** Our goal is now to complete the resonance curves (see Figure 4, right) in the SO regime by computing the torus solutions amplitudes. To this end, we use the software Knut (see Schilder, Osinga, & Vogt, 2005) to compute the torus solutions emerging from the Hopf bifurcations for equation 3.4. The torus solutions have two intrinsic frequencies  $\frac{\omega_F}{2\pi}$ ,  $\frac{\omega_{app}}{2\pi}$ , which generate the toroidal dynamics. When the rotation number  $\omega_{app}/\omega_F$  is rational, the torus becomes a periodic solution: this happens at the tip of the Arnold tongues. In Figure 10, we plot the PL amplitude and the torus amplitude as functions of the forcing frequency  $\omega_F$ . An example of torus response is shown in Figure 10,

bottom left. A PL response is shown in Figure 10, top left. A PL solution (close to the peak 1:2) with frequency  $\frac{\omega_H}{2\pi}$  and forcing frequency  $\frac{2\omega_H}{2\pi}$  is shown in Figure 10, bottom right; this is the period-doubling phenomenon that was examined earlier. Finally, we have also plotted, with triangles, points where the rotation number is  $\frac{1}{4}$  (labeled R4),  $\frac{1}{3}$  (labeled R3) and  $\frac{1}{2}$  (labeled R2). An example of a PL solution with frequency  $\omega_F/3$  is shown in Figure 10, bottom left. This solution is very unstable and requires careful adjustment of the forcing frequency; otherwise a torus solution appears.

#### 4 Discussion

---

We have analyzed networks regimes that are important for understanding phase-amplitude coupling, which is relevant for communication between the hippocampus and the entorhinal cortex, for example (Jensen & Colgin, 2007; Igarashi et al., 2014). More precisely, we restricted our analysis to the periodic forcing of a specific class of inhibition-stabilized E-I networks, working close to a Hopf bifurcation. The results apply to a mean field description of a population of neurons, and as such, most of our results should carry over to spiking neural networks in an ISN regime. Also, the results are insensitive to synaptic delays (Roxin, Brunel, & Hansel, 2005; Coombes & Laing, 2008) as long as the network is close to a Hopf bifurcation.

Some predictions can be made based on the results of our analysis. First, ISNs require the tuning of an E-I network close to a Hopf bifurcation effectively acting as a Stuart-Landau oscillators. Working close to a Hopf bifurcation can lead to interesting phenomena that depend mainly on the value of the shear  $\gamma$  and whether the network is tuned to the ISN regime. In short, the ISN regime can produce only phase-locked solutions and hysteresis of phase-locked solutions when periodically forced. In contrast, networks that support sustained oscillations (such as the ones induced by carbachol in Akam et al., 2012) are likely to produce torus responses when periodically forced. The shear breaks the symmetry of the 1:1 resonance peak (see section 3.5.1), which makes periodic forcing of neural networks a flawed tool to determine the intrinsic gamma frequency (Akam et al., 2012). An extreme example of this is shown in Figure 11, where the shear governs the emergence of multistability.

Another prediction of the resonance curve is that the main resonance peaks arise at  $\frac{1}{2}$ , 1, 2 times the network intrinsic frequency which reflects the large amplification of the input component located near these peaks (see Ray & Maunsell, 2011). One interesting fact is that the resonance curves of the ISN networks are more isolated because they cannot produce torus responses (compare Figure 10 with Figure 4, left). In particular, the ISN response to a broadband signal corresponds to a nonlinear and highly selective filter at 1, 2,  $\frac{1}{2}$  times its intrinsic frequency  $\omega_H$ . In comparison, the network with sustained oscillations will mix all frequency in a very complicated manner because of the torus responses.

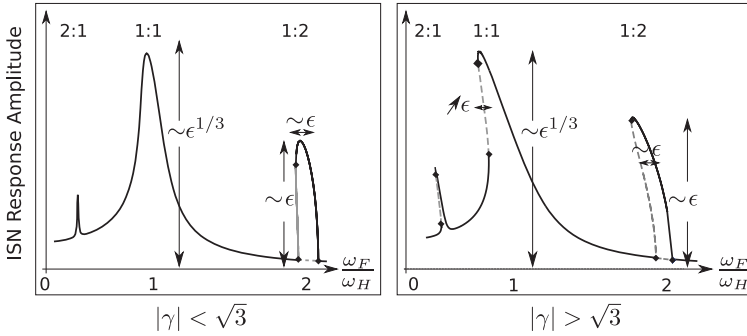


Figure 11: Plot of the resonance curves in the ISN regime for two different shears  $\gamma$ . The scaling of the width and amplitude of the peaks is indicated as a function of the forcing amplitude  $\epsilon$ . The domain of multistability for  $|\gamma| > \sqrt{3}$  is a decreasing function of  $\epsilon$  but an increasing function of  $\gamma$ . The amplitude of the 1:1 peak does not scale exactly as  $\epsilon^{1/3}$  as indicated. For more details, see the text and appendix F.

We summarize these results in Figure 11 for the ISN regime and for two different ranges of shears ( $\gamma$ ) that lead to the two different classes of resonance curves. The larger the shear  $|\gamma| > \sqrt{3}$ , the larger the region of multistability. The first prediction is that in the ISN regime, the network response frequency is the same as the forcing frequency except near the 1:2 peak, where it is half the forcing frequency. This period doubling phenomenon also works in the case of a network that supports sustained oscillations. The second set of predictions concerns the scaling of the different peaks as functions of the forcing amplitude  $\epsilon$ , as shown in Figure 11. As such, the resonance curve and the scaling of its peaks constitute an experimental indirect proof of an ISN working regime that can be tested using optogenetics experiments.

Most of these effects have been overlooked in studies focused on synchronization and phase locking (Hoppensteadt & Izhikevich, 1997; Izhikevich, 2007) with notable exceptions (Vierling-Claassen & Kopell, 2009). The widely used theory of weakly connected Hopf oscillations (WCHO) presented in Hoppensteadt and Izhikevich (1997, theorem 5.10) ignores resonance effects and considers only phase coupling. In our view, the resonant normal form is the one that should be perturbed using the perturbation  $\delta\omega$  when considering weakly connected oscillators, not the Hopf normal form used in Hoppensteadt and Izhikevich (1997). In particular, the normal form for the external forcing of WCHO (Hoppensteadt & Izhikevich, 1997, theorem 5.8) leads to the incorrect conclusion that the resonant frequency affects only linear terms (see equation 3.4).

In a more recent study (Ostojic, Brunel, & Hakim, 2009), the second resonance peak was missed because the authors consider an ansatz for the

response at frequency  $2\omega_H$  when the network is forced at  $2\omega_H$ , whereas the maximum response amplitude occurs at frequency  $\omega_F$  based on our results. This was also overlooked in Cardin et al. (2009) because the authors extracted only from the network response, the frequency component around the forcing frequency  $\omega_F$ , possibly throwing away the main frequency component around  $\omega_F/2$  when the forcing frequency is at twice the gamma-peak frequency. A recent computational study (Hahn, Bujan, Frégnac, Aertsen, & Kumar, 2014) seems to indicate the presence of the second resonance peak (see Figure 4.b in that paper). It would be interesting to understand the link with the ISN working regime used in this work.

Periodic forcing of a supercritical Hopf bifurcation for single neuron dynamics is rare and consequently has not been studied. Indeed, class II neurons work close to a subcritical Hopf bifurcation with a fold on the limit cycle branch (Izhikevich, 2007). This suggests that periodic forcing of the generalized Hopf bifurcation (also called a Bautin bifurcation) is relevant for resonance effects in class II neurons and should be more closely examined.

A central result of this study is that an ISN requires the network to be close to a Hopf bifurcation. Hence, the predicted properties of this working regime can be experimentally tested. The normal form method (Haragus & Iooss, 2011) can be applied to study networks close to other local bifurcations such as the Bogdanov-Takens bifurcation. In the study of periodic forcing and quasiperiodic forcing, we expect the general form of the resonance curves to remain if there is dominant frequency in the forcing (Saleh & Wager, 2010).

As suggested in Golubitsky et al. (2009), feedforward chains of  $n$  ISN networks are highly selective to the forcing frequency as the maximum of the 1:1 peak, for the  $n$ th network, is  $\epsilon^{1/3^n}$  (other peaks have similar power laws). Thus, these feedforward chains would be very useful for extracting frequency components of noisy inputs by working as nonlinear filters and would be able, at the same time, to demultiplex the main components of the input. We plan to examine this effect in feedback networks.

We also plan to explore the effects of adding noise to the periodic forcing, which should exhibit stochastic resonance phenomena. Indeed, one of the first studies of stochastic resonance (Benzi, Sutera, & Vulpiani, 1981) considered the periodic forcing of a pitchfork bifurcation with noise perturbation, which led to multistability of PL solutions. When multistable PL solutions are perturbed with noise, they exhibit stochastic resonance. Similarly, the periodic forcing of the Hopf bifurcation with large enough shear should also exhibit multistability, which is the main ingredient in Benzi et al. (1981).

## Appendix A: Normal Form Computation of the 1:1 Resonance

Notation for hermitian scalar products for vectors and functions:  $\langle V, W \rangle \stackrel{\text{def}}{=} V_1 \overline{W_1} + V_2 \overline{W_2}$  and  $\langle f, g \rangle_{\text{per}, \tau} \stackrel{\text{def}}{=} \frac{1}{\tau} \int_0^\tau \langle f(t), g(t) \rangle dt$ .

We call  $\zeta$  and  $\zeta^*$  the eigenvector of the Jacobian and the Jacobian adjoint at the equilibrium, respectively, for the eigenvalues  $i\omega_H$  and  $-i\omega_H$  with the normalization  $\langle \zeta, \zeta^* \rangle = 1$ .

**Proposition 1.** *The normal form of equation 2.1 for the 1:1 resonance is*

$$\dot{z} = z(a\delta\theta^{(0)} + i(\omega_H - \omega_F) - b|z|^2) + c_2\epsilon$$

plus additional terms  $o(|z|^3 + |\epsilon| + |z|(|\epsilon| + |\delta\theta|))$  where  $c_2 = \frac{1}{2}\langle \theta^{(1)} | dS(V^f + \theta^{(0)}) \rangle, \zeta^*$  and  $b$  is defined in equation 3.2.

**Proof.** In order to apply the result (Haragus & Iooss, 2011, III.5.2), we need the forcing frequency to be constant. Hence, we start by rescaling the time variable  $s \stackrel{\text{def}}{=} \omega_F t$ , which yields

$$\begin{aligned} \frac{d}{ds}V &= \frac{1}{\omega_F}[-V + S(\mathbf{J} \cdot V + \theta^{(0)} + \epsilon\theta^{(1)} \cos(s))] \\ &= \frac{1 - \omega}{\omega_H}[-V + S(\mathbf{J} \cdot V + \theta^{(0)} + \epsilon\theta^{(1)} \cos(s))], \end{aligned}$$

where  $\frac{\omega_F}{\omega_H} = \frac{1}{1-\omega}$ . The bifurcation parameters are  $\mu = (\theta^{(0)}, \epsilon, \omega)$  and the bifurcation point is  $\mu_c = (\theta_H^{(0)}, 0, 0)$ ,  $V = V^f$ . It follows that the Hopf frequency is  $2\pi$  at the bifurcation point  $\mu = \mu_c$ . We write  $V(s) = V^f + v_0(s) + \Psi(v_0(s); \theta^{(0)}, \epsilon, \omega, s)$  where  $\Psi(0; \theta_H^{(0)}, 0, 0, s) = 0$ ,  $D_1\Psi(0; \theta_H^{(0)}, 0, 0, s) = 0$  and  $\Psi$  is  $2\pi$ -periodic in  $s$ . From Haragus and Iooss (2011, III.5.2), we have  $v_0(s) = A(s)\zeta + c.c.$  and

$$\begin{aligned} \dot{A} &= iA + a(\theta^{(0)}, \epsilon, \omega)A + c(\theta^{(0)}, \epsilon, \omega)e^{is} + e(\theta^{(0)}, \epsilon, \omega)A^2e^{-is} \\ &\quad + f(\theta^{(0)}, \epsilon, \omega)\bar{A}^2e^{3is} + b(\theta^{(0)}, \epsilon, \omega)|A|^2A + g(\theta^{(0)}, \epsilon, \omega)A^3e^{-2is} \\ &\quad + h(\theta^{(0)}, \epsilon, \omega)\bar{A}^3e^{4is} + j(\theta^{(0)}, \epsilon, \omega)\bar{A}|A|^2e^{2is}, \end{aligned}$$

where  $a(\mu_c) = c(\mu_c) = d(\mu_c) = 0$ . As the expression  $G(V; \mu, s)$  of  $\frac{d}{ds}V$  given by  $G(V; \mu, s) = \frac{1-\omega}{\omega_H}[-V + S(\mathbf{J} \cdot V + \theta^{(0)} + \epsilon\theta^{(1)} \cos(s))]$  satisfies  $\partial_s G(V; \mu_c, t) = 0$ , all the coefficients with an exponential factor vanish at  $\mu = \mu_c$  (see Haragus & Iooss, 2011, III.5.2), hence at order  $o(|A|^3 + |\mu| + |A\mu| + |A|)$ ,

$$\frac{dA}{ds} = iA + a(\theta^{(0)}, \epsilon, \omega)A + c(\theta^{(0)}, \epsilon, \omega)e^{is} + b(\theta_H^{(0)}, 0, 0)|A|^2A.$$

Finally, writing  $A(s) = z(s)e^{is}$ , we find

$$\frac{dz}{ds} = (a(\theta^{(0)}, \epsilon, \omega) + b(\theta_H^{(0)}, 0, 0)|z|^2)z + c(\theta^{(0)}, \epsilon, \omega).$$

We now compute the coefficients  $a(\theta^{(0)}, \epsilon, \omega)$ ,  $c(\theta^{(0)}, \epsilon, \omega)$  as a linear expression of the parameters  $(\theta^{(0)} - \theta_H^{(0)}, \epsilon, \omega)$  and also the coefficient  $b$ . First, Taylor-expand the function  $\Psi$ :

$$\Psi(v_0; \mu) = \sum_{l_1+l_2+r>1} A^{l_1} \bar{A}^{l_2} \mu^r \tilde{\Psi}_{l_1, l_2, r}.$$

Using equation 5.5 in Haragus and Iooss (2011) for the normal form change of variable  $\Psi$  and Fourier series, we find

$$\begin{cases} \frac{\partial a}{\partial \mu} = \langle G_{11}(\zeta) + 2G_{20}(\zeta, \Psi_{001}), \zeta^* \rangle_{per, 2\pi}, \\ \frac{\partial c}{\partial \mu} = \langle G_{01}(\zeta), e^{-is} \zeta^* \rangle_{per, 2\pi}, \\ b(\mu_c) = \langle 2G_{20}(\zeta, \Psi_{110}) + 2G_{20}(\zeta, \bar{\Psi}_{200}) + 3G_{30}(\zeta, \zeta, \bar{\zeta}), \zeta^* \rangle_{per, 2\pi}, \end{cases} \tag{A.1}$$

where  $G_{ij} \stackrel{def}{=} \frac{\partial^{i+j} G}{\partial^i V \partial^j \mu}$ . It is straightforward to check that the expression of  $b$  is the same as for the case of a regular Hopf bifurcation without forcing (Kuznetsov, 2004; Haragus & Iooss, 2011). Hence, we have

$$b(\theta_H^{(0)}, 0, 0) = \frac{-b}{\omega_H}.$$

Let  $G_{01} = \frac{d\epsilon}{\omega_H} DS \theta^{(1)} \cos(s) + \frac{d\theta^{(0)}}{\omega_H} DS + 0 \cdot d\omega$  with  $DS \stackrel{def}{=} DS(\mathbf{J} \cdot V^f + \theta_H^{(0)})$ . Indeed, the derivative with regard to  $\omega$  vanishes at  $V = V^f$ ,  $\mu = \mu_c$ , and this gives the coefficient

$$c(\mu - \mu_c) = \frac{\epsilon}{2\omega_H} \langle DS \theta^{(1)}, \zeta^* \rangle. \tag{A.2}$$

Let us focus now on the linear coefficient  $a(\mu - \mu_c)A$ . We start with the expression of  $G_{20}$ ,

$$G_{20}(U_1, U_2) = D^{(2)}S(\mathbf{J} \cdot V^f + \theta_H^{(0)})(\mathbf{J} \cdot U_1)(\mathbf{J} \cdot U_2),$$

which is time  $s$  independent. The equation for  $\Psi_{001}$  is

$$\frac{d}{ds}\Psi_{001} - \mathbf{L}\Psi_{001} = G_{01},$$

where  $\mathbf{L}$  is the Jacobian at  $V = V^f$ . Using Fourier series  $G_{01} = \sum_{n=-\infty}^{\infty} G_{01}^{(n)} e^{ins}$  and  $\Psi_{001} = \sum_{n=-\infty}^{\infty} \Psi_{001}^{(n)} e^{ins}$ , we find

$$(in - \mathbf{L}) \Psi_{001}^{(n)} = G_{01}^{(n)}, \quad \forall n \in \mathbb{Z}.$$

From the expression of  $G_{20}$  and the scalar product  $\langle G_{20}(\zeta, \Psi_{001}), \zeta^* \rangle_{per, 2\pi}$  in the expression of  $a(\mu - \mu_c)$ , it appears that only the term  $\langle G_{20}(\zeta, \Psi_{001}^{(0)}), \zeta^* \rangle_{per, 2\pi}$  is nonvanishing. This gives  $-\langle G_{20}(\zeta, \mathbf{L}^{-1}G_{01}^{(0)}), \zeta^* \rangle_{per, 2\pi}$ . Also from the expression of  $G_{01}$ ,

$$G_{11} = -\frac{d\omega}{\omega_H} \mathbf{L} + \frac{d\theta^{(0)}}{\omega_H} D^{(2)} \mathbf{S} \mathbf{J} + \frac{d\epsilon}{\omega_H} \theta^{(1)} \cos(s) D^{(2)} \mathbf{S} \mathbf{J},$$

$$D^{(2)} \mathbf{S} \stackrel{def}{=} D^{(2)} \mathbf{S} (\mathbf{J} \cdot V^f + \theta_H^{(0)}).$$

This allows us to find an expression for  $a(\mu - \mu_c)$  using  $\langle \mathbf{L}\zeta, \zeta^* \rangle = i\omega_H$ :

$$a(\mu - \mu_c) = -i\omega + \frac{\delta\theta^{(0)}}{\omega_H} ((D^{(2)} \mathbf{S} \mathbf{J} \cdot \zeta - 2G_{20}(\zeta, \mathbf{L}^{-1}G_{01}^{(0)}), \zeta^*)_{per, 2\pi}).$$

The second term is the same as for the case of no forcing (Kuznetsov, 2004; Haragus & Iooss, 2011); hence we find

$$a(\mu - \mu_c) = -i\omega + \frac{\delta\theta^{(0)}}{\omega_H} a.$$

where  $a$  is defined in equation 3.2. To sum up, we have found that

$$\frac{d}{ds} A = \left( 1(1 - \omega) + \frac{\delta\theta^{(0)}}{\omega_H} a \right) A - \frac{b}{\omega_H} |A|^2 A + \frac{\epsilon}{2\omega_H} \langle DS \theta^{(1)}, \zeta^* \rangle e^{is}$$

or

$$\frac{d}{ds} z = \left( -1\omega + \frac{\delta\theta^{(0)}}{\omega_H} a \right) z - \frac{b}{\omega_H} |z|^2 z + \frac{\epsilon}{2\omega_H} \langle DS \theta^{(1)}, \zeta^* \rangle.$$

Coming back to the original time  $\frac{d}{dt} = \omega_F \frac{d}{ds} = \frac{\omega_H}{1-\omega} \frac{d}{ds}$ , we find

$$\frac{d}{dt}z = \left(-1\omega\omega_F + \frac{\delta\theta^{(0)}}{1-\omega}a\right)z - \frac{b}{1-\omega}|z|^2z + \frac{\epsilon}{2(1-\omega)}\langle DS\theta^{(1)}, \zeta^* \rangle,$$

which gives at order  $o(|\mu| + |\mu z|)$

$$\frac{d}{dt}z = (1(\omega_H - \omega_F) + \delta\theta^{(0)}a)z - b|z|^2z + \frac{\epsilon}{2}\langle DS\theta^{(1)}, \zeta^* \rangle.$$

**Appendix B: Normal Form Computation of the 1:2 Resonance** \_\_\_\_\_

**Proposition 2.** *The normal form for the 1:2 resonance is*

$$\dot{z} = z(a\delta\theta^{(0)} + 1(\omega_H - \omega_F/2) - b|z|^2) + c_2\bar{z}$$

where  $c_2 = \frac{\epsilon}{2}\langle D^{(2)}S\theta^{(1)}\mathbf{J} \cdot \zeta + 2G_{20}(\zeta, (21\omega_H - \mathbf{L})^{-1}DS\theta^{(1)}, \zeta^*)$  and  $b$  is defined in equation 3.2.

**Proof.** The proof in appendix A shows that we only need to consider the case  $\omega_F = 2\omega_H$  and incorporate the perturbation parameter  $\omega$  as a linear term where  $\frac{\omega_F}{\omega_H} = \frac{1}{\frac{1}{2}-\omega}$ . Hence,

$$c_2 = \epsilon\langle G_{11}(\zeta) + 2G_{20}(\zeta, \Psi_{001}), e^{-2i\omega_H t} \zeta^* \rangle_{per, 2\pi/\omega_F},$$

which gives

$$c_2 = \frac{1}{2}\epsilon\langle D^{(2)}S\theta^{(1)}\mathbf{J} \cdot \zeta + 2G_{20}(\zeta, \Psi_{001}^{(1)}), \zeta^* \rangle,$$

where  $\Psi_{001} = \sum_n \Psi_{001}^{(n)} e^{2i\omega_H n t}$  and

$$c_2 = \frac{\epsilon}{2}\langle D^{(2)}S\theta^{(1)}\mathbf{J} \cdot \zeta + 2G_{20}(\zeta, (21\omega_H - \mathbf{L})^{-1}DS\theta^{(1)}), \zeta^* \rangle.$$

**Appendix C: Hopf Bifurcation Curve Near the 1:1 Resonance** \_\_\_\_\_

**Lemma 1.** *When  $\Re(a)\delta\theta_1^{(0)} < 0$ , the resonance curve does not intersect the Hopf bifurcation curve.*

**Proof.** In order to simplify, let us assume  $\Re b = 1$  and write the 1:1 normal form (after a scaling in  $z$  to transform  $c_2 \rightarrow |c_2|$ )

$$\dot{z} = z(\lambda + i\omega - (1 + i\gamma)|z|^2) + |c_2|,$$

where we have written  $\omega = \delta\omega + \Im a\delta\theta_1^{(0)}$ ,  $\lambda = \Re a\delta\theta_1^{(0)}$ , and  $\gamma$  is the shear. The Hopf bifurcation curve is computed using two conditions (Kuznetsov, 2004) regarding the Jacobian  $\mathbf{L}$  of the above dynamical system:  $\det(\mathbf{L}) > 0$ ,  $\text{tr}(\mathbf{L}) = 0$ , which satisfies

$$\frac{1}{2}\omega^2\lambda - \frac{1}{2}\lambda^2\gamma\omega + \frac{1}{8}(\gamma^2 + 1)\lambda^3 - |c_2|^2 = 0.$$

There is a solution  $\omega$  if and only if  $\lambda(8|c_2|^2 - \lambda^3) > 0$ . This condition is not satisfied when  $\lambda < 0$ .

**Appendix D: Simplification of the 1:1 Normal Form** \_\_\_\_\_

**Lemma 2.** *If  $\Re b > 0$ ,  $\Im b > 0$  and  $\delta\theta_1^{(0)}(\Re a + \gamma\Im a) + \gamma\delta\omega \neq 0$ , then the equation  $\dot{z} = z(a\delta\theta_1^{(0)} + i\delta\omega - b|z|^2)z + c_2$  is equivalent to the equation*

$$\dot{z} = z(\epsilon_0 + i\tau - |z|^2)ze^{i\arg(b)} + \rho, \tag{D.1}$$

where  $\epsilon_0 = \text{sign}(\delta\theta_1^{(0)}(\Re a + \gamma\Im a) + \gamma\delta\omega)$ ,  $\tau = \frac{\delta\omega + \delta\theta_1^{(0)}(\Im a - \gamma\Re a)}{|\gamma\delta\omega + \delta\theta_1^{(0)}(\Re a + \gamma\Im a)|}$  and  $\rho = \frac{|c_2||b|^2}{|\Re b|^{3/2} \cdot |(\Re a + \gamma\Im a)\delta\theta_1^{(0)} + \gamma\delta\omega|^{3/2}}$ .

**Proof.** For the scaling:  $z \rightarrow ze^{-i\arg c_2}$ , this implies  $c_2 \rightarrow |c_2|$ . For the scaling:  $t \rightarrow Rt$  and  $z \rightarrow Az$  with appropriate  $A, R$ , this implies  $\epsilon_0 = \text{sign}\Re \frac{a\delta\theta_1^{(0)} + i\delta\omega}{b}$ ,  $\tau = \Im \frac{a\delta\theta_1^{(0)} + i\delta\omega}{b} \left| \Re \frac{a\delta\theta_1^{(0)} + i\delta\omega}{b} \right|^{-1}$  and  $\rho = \frac{|c_2|}{|b| \cdot \left| \Re \frac{a\delta\theta_1^{(0)} + i\delta\omega}{b} \right|^{3/2}}$ .

Recall that  $\cos \arg(b) > 0$  because the Hopf bifurcation is supercritical. Then  $\epsilon_0 = \text{sign}\Re \left( \frac{a\delta\theta_1^{(0)} + i\delta\omega}{b} \right) = \text{sign}(\cos \arg(b) \frac{\delta\theta_1^{(0)}\Re a + \gamma\delta\theta_1^{(0)}\Im a + \gamma\delta\omega}{|b|(1+\gamma^2)}) = \text{sign}(\delta\theta_1^{(0)}(\Re a + \gamma\Im a) + \gamma\delta\omega)$ . Expressions for  $\tau$  and  $\rho$  follow accordingly:

$$\tau = \Im \left( \frac{a\delta\theta_1^{(0)} + i\delta\omega}{b} \right) \Big/ \Re \left( \frac{a\delta\theta_1^{(0)} + i\delta\omega}{b} \right),$$

$$\rho = |c_2|/|b| \cdot \left| \Re \frac{a\delta\theta_1^{(0)} + i\delta\omega}{b} \right|^{3/2}.$$

**Appendix E: Equation of the Resonance Curve in the Plane  $(\tau, \rho)$**  \_\_\_\_\_

**Corollary 1.** *From appendix D, the parameters satisfy*

$$\rho^{2/3} = \frac{\Im(b)}{\Re(a)\delta\theta_1^{(0)}} \left( \frac{|c_2|}{|b|} \right)^{2/3} \left( \frac{\epsilon_0}{\gamma} - \tau \right), \quad c_2 \stackrel{def}{=} \frac{\epsilon}{2} (DS \theta_1^{(1)}, \zeta^*), \quad (E.1)$$

assuming that the Hopf bifurcation is supercritical (i.e.,  $\Re(b) > 0$ ).

**Proof.** We first compute  $\frac{\epsilon_0}{\gamma} - \tau = \frac{\Re(a)\delta\theta_1^{(0)}(\gamma + \frac{1}{\gamma})}{|\gamma\delta\omega + \delta\theta_1^{(0)}(\Re a + \gamma\Im a)|}$  and  $(\frac{\rho}{|c_2| |b|^2})^{2/3} = \frac{1}{|\Re b| \cdot |\gamma\delta\omega + \delta\theta_1^{(0)}(\Re a + \gamma\Im a)|}$ , which gives

$$\begin{aligned} \frac{\epsilon_0}{\gamma} - \tau &= \left( \frac{\rho |b|}{|c_2|} \right)^{2/3} [\Re(a)\delta\theta_1^{(0)}] \left( \gamma + \frac{1}{\gamma} \right) \frac{|\Re(b)|}{|b|^2} \\ &= \left( \frac{\rho |b|}{|c_2|} \right)^{2/3} [\Re(a)\delta\theta_1^{(0)}] \frac{\text{sign}(\Re b)}{\Im(b)}. \end{aligned}$$

Using the fact that  $\Re(b) > 0$  allows us to conclude the proof.

**Appendix F: Properties of the PL Solutions Around the 1:2 Resonance** —

**Lemma 3.** *We show here that the 1:2 resonance peak has the following properties:*

1. *The peak exists if and only if  $|c_2|^2 > (\Re a \delta\theta_1^{(0)})^2$ , that is, if the forcing amplitude is large enough.*
2. *The width at its base is  $2\sqrt{|c_2|^2 - \lambda^2}$ . Hence, it scales as the amplitude  $\epsilon$  since  $c_2$  is proportional to the forcing amplitude.*
3. *Its height is  $|c_2| + \Re a \delta\theta_1^{(0)} > 0$ .*

**Proof.** Let us define  $\lambda \stackrel{def}{=} \Re a \delta\theta_1^{(0)}$  and  $\omega \stackrel{def}{=} \Im a \delta\theta_1^{(0)} + \omega_H - \omega_F/2$ . Using the scaling  $z \rightarrow ze^{-i \arg c_2/2}$ , we can replace  $c_2$  by its modulus. PL solutions are solutions to the equation

$$z(a\delta\theta_1^{(0)} + i(\omega_H - \omega_F/2) - b|z|^2) + c_2\bar{z} = 0,$$

which gives  $z = 0$  or  $(1 + \gamma^2)Y^2 - 2(\lambda + \omega\gamma)Y + (\lambda^2 - |c_2|^2 + \omega^2) = 0$ , where  $Y \stackrel{def}{=} \Re b X$  and  $X \stackrel{def}{=} |z|^3$ . The width at its base given by the difference of the  $\omega$  such that  $Y = 0$  is the solution. These  $\omega$  satisfy  $\lambda^2 - |c_2|^2 + \omega^2$ , which gives the width  $2\sqrt{|c_2|^2 - \lambda^2}$ . It is positive only if  $|c_2|^2 > \lambda^2$ . Hence, this proves properties 1 and 2.

From the implicit function theorem, the maximum  $Y_m$  of  $Y$  as function of  $\omega$  occurs for a value  $\omega_m$  such that  $\omega_m = \gamma Y_m$ . Result 3 in lemma 3 follows by inserting this last expression in the quadratic equation:  $Y_m = \lambda + |c_2| > 0$ .

**Appendix G: Dynamics Around the 1:2 Resonance Peak** \_\_\_\_\_

We characterize here the dynamics of the 1:2 resonance in the ISN regime,  $\Re a\delta\theta_1^{(0)} < 0$ . We show that no torus solutions are possible and that there are one, three, or five PL solutions.

**Lemma 4.** *In the ISN regime (i.e., when  $\Re a\delta\theta_1^{(0)} < 0$ ), no torus solutions are possible. There are one, three, or five PL solutions.*

**Proof.** We first simplify the 1:2 normal form using successive rescalings. Using the scaling  $z \rightarrow ze^{-i\arg c_2/2}$ , we can replace  $c_2$  by its modulus. Then, using a real scaling  $z \rightarrow z/\sqrt{|b|}$ , we can assume  $|b| = 1$ . Hence, we can assume that we have  $\dot{z} = z((a\delta\theta_1^{(0)} + i(\omega_H - \omega_F/2))e^{-i\arg b} - |z^2|)e^{i\arg b} + |c_2|z$ . Finally, using the scalings  $z \rightarrow z/\sqrt{|c_2|}$  and  $t \rightarrow |c_2|t$ , we arrive at the equation

$$\dot{z} = z(\sigma + i\tau - |z^2|)e^{i\arg b} + \bar{z}$$

where  $\sigma + i\tau = (a\delta\theta_1^{(0)} + i(\omega_H - \omega_F/2))e^{-i\arg b}/|c_2|$ . A resonance curve parameterized by  $\omega_F$  describes a line in the plane  $(\tau, \sigma)$  given by

$$\tau = \gamma\sigma + (1 + \gamma^2)\Re(a\delta\theta_1^{(0)})\frac{\Re b}{|b|^2}.$$

Hence, in the ISN regime ( $\Re a\delta\theta_1^{(0)} < 0$ ), this line is below the Hopf curve (H),  $\tau = \gamma\sigma$ , in the parameter plane (see Gambaudo, 1985). This shows that the ISN regime can produce only the phase diagrams 1, 5, or 4 in Gambaudo (1985), all of which are composed solely of fixed points.

**Acknowledgments** \_\_\_\_\_

We thank Frank Schilder and Robert Szalai for their help in computing the torus solutions. We warmly thank Antonio Pinto-Duarte for his valuable comments on the manuscript.

This work was partially supported by the European Union Seventh Framework Programme (FP7/2007-2013) under grant agreement 269921 (BrainScaleS), 318723 (Mathematics), by the ERC advanced grant NerVi 227747, and by the Human Brain Project (HBP). The Swartz Foundation and the Howard Hughes Medical Institute also provided support.

## References

---

- Akam, T., & Kullmann, D. M. (2010). Oscillations and filtering networks support flexible routing of information. *Neuron*, *67*(2), 308–320.
- Akam, T., Oren, I., Mantoan, L., Ferenczi, E., & Kullmann, D. M. (2012). Oscillatory dynamics in the hippocampus support dentate gyrus-CA3 coupling. *Nature Neuroscience*, *15*(5), 763–768.
- Arnold, V. I. (1988). *Geometrical methods in the theory of ordinary differential equations*. New York: Springer.
- Aronson, D., Ermentrout, B., & Kopell, N. (1990). Amplitude response of coupled oscillators. *Physica D*, *41*, 403–449.
- Bartos, M., Vida, I., & Jonas, P. (2007). Synaptic mechanisms of synchronized gamma oscillations in inhibitory interneuron networks. *Nature Reviews Neuroscience*, *8*(1), 45–56.
- Benzi, R., Sutera, A., & Vulpiani, A. (1981). The mechanism of stochastic resonance. *Journal of Physics A: Mathematical and General*, *14*(11), L453.
- Bichot, N. P., Rossi, A. F., & Desimone, R. (2005). Parallel and serial neural mechanisms for visual search in macaque area V4. *Science*, *308*(5721), 529–534.
- Borisjuk, G. N., Borisjuk, R. M., Khibnik, A. I., & Roose, D. (1995). Dynamics and bifurcations of two coupled neural oscillators with different connection types. *Bulletin of Mathematical Biology*, *57*(6), 809–840.
- Borisjuk, R. M., & Kirillov, A. B. (1992). Bifurcation analysis of a neural network model. *Biological Cybernetics*, *66*(4), 319–325.
- Buzsaki, G. (2004). Neuronal oscillations in cortical networks. *Science*, *304*(5679), 1926–1929.
- Buzsaki, G., & Chrobak, J. J. (1995). Temporal structure in spatially organized neuronal ensembles: A role for interneuronal networks. *Current Opinion in Neurobiology*, *5*(4), 504–510.
- Cardin, J. A., Carl, M., Meletis, K., Knoblich, U., Zhang, F., Deisseroth, K., ... Moore, C. I. (2009). Driving fast-spiking cells induces gamma rhythm and controls sensory responses. *Nature*, *459*(7247), 663–667.
- Colgin, L. L., Denninger, T., Fyhn, M., Hafting, T., Bonnevie, T., Jensen, O., ... Moser, E. I. (2009). Frequency of gamma oscillations routes flow of information in the hippocampus. *Nature*, *462*(7271), 353–357.
- Coombes, S., & Laing, C. (2008). Delays in activity based neural networks. *Philosophical Transactions of the Royal Society A*, *367*, 1117–1129.
- Decker, R., & Noonburg, V. W. (2012). A periodically forced Wilson-Cowan system with multiple attractors. *SIAM Journal on Mathematical Analysis*, *44*(2), 887–905.
- Elphick, C., Iooss, G., & Tirapegui, E. (1987). Normal form reduction for time-periodically driven differential equations. *Physics Letters A*, *120*(9), 459–463.
- Ermentrout, G. B. (1981).  $n:m$  Phase-locking of weakly coupled oscillators. *Journal of Mathematical Biology*, *12*(3), 327–342.
- Ermentrout, G. B., & Terman, D. H. (2010). *Mathematical foundations of neuroscience*. New York: Springer.
- Gambaudo, J. M. (1985). Perturbation of a Hopf bifurcation by an external time-periodic forcing. *Journal of Differential Equations*, *57*, 172–199.

- Golubitsky, M., Shiau, L., Postlethwaite, C., & Zhang, Y. (2009). The feed-forward chain as a filter-amplifier motif. In K. Josic, J. Rubin, M. Matias, & R. Romo (Eds.), *Coherent behavior in neuronal networks* (pp. 95–120). New York: Springer.
- Guckenheimer, J., & Holmes, P. (1983). *Nonlinear oscillations, dynamical systems, and bifurcations of vector fields*. New York: Springer.
- Hahn, G., Bujan, A. F., Frégnac, Y., Aertsen, A., & Kumar, A. (2014). Communication through resonance in spiking neuronal networks. *PLoS Computational Biology*, 10(8), e1003811.
- Haragus, M., & Iooss, G. (2011). *Local bifurcations, center manifolds, and normal forms in infinite-dimensional dynamical systems*. London: Springer.
- Hemptonne, C. d., Ryapolova-Webb, E. S., Air, E. L., Garcia, P. A., Miller, K. J., Ojemann, J. G., . . . Starr, P. A. (2013). Exaggerated phase amplitude coupling in the primary motor cortex in Parkinson disease. *Proceedings of the National Academy of Sciences*, 110(12), 4780–4785.
- Hoppensteadt, F. C., & Izhikevich, E. M. (1997). *Weakly connected neural networks*. New York: Springer.
- Igarashi, K. M., Lu, L., Colgin, L. L., Moser, M.-B., & Moser, E. I. (2014). Coordination of entorhinal-hippocampal ensemble activity during associative learning. *Nature*, 510(7503), 143–147.
- Izhikevich, E. M. (2007). *Dynamical systems in neuroscience: The geometry of excitability and bursting*. Cambridge, MA: MIT Press.
- Jadi, M. P., & Sejnowski, T. J. (2014a). Cortical oscillations arise from contextual interactions that regulate sparse coding. *Proceedings of the National Academy of Sciences*, 111(18), 6780–6785.
- Jadi, M. P., & Sejnowski, T. J. (2014b). Regulating cortical oscillations in an inhibition-stabilized network. *Proceedings of the IEEE*, 102(5), 830–842.
- Jensen, O., & Colgin, L. L. (2007). Cross-frequency coupling between neuronal oscillations. *Trends in Cognitive Sciences*, 11(7), 267–269.
- Kang, K., Shelley, M., Henrie, J. A., & Shapley, R. (2010). LFP spectral peaks in V1 cortex: Network resonance and cortico-cortical feedback. *Journal of Computational Neuroscience*, 29(3), 495–507.
- Kuznetsov, I. A. (2004). *Elements of applied bifurcation theory*, 3rd ed. New York: Springer.
- Ledoux, E., & Brunel, N. (2011). Dynamics of networks of excitatory and inhibitory neurons in response to time-dependent inputs. *Frontiers in Computational Neuroscience*, 5.
- Lewis, D. A., Hashimoto, T., & Volk, D. W. (2005). Cortical inhibitory neurons and schizophrenia. *Nature Reviews Neuroscience*, 6(4), 312–324.
- Murphy, B. K., & Miller, K. D. (2009). Balanced amplification: A new mechanism of selective amplification of neural activity patterns. *Neuron*, 61(4), 635–648.
- Neu, J. C. (1979). Coupled chemical oscillators. *SIAM Journal on Applied Mathematics*, 37(2), 307–315.
- Newhouse, S., Ruelle, D., & Takens, F. (1978). Occurrence of strange axiom A attractors near quasi periodic flows on  $T^m$ ,  $m \geq 3$ . *Communications in Mathematical Physics*, 64(1), 35–40.

- Ostojic, S., Brunel, N., & Hakim, V. (2009). Synchronization properties of networks of electrically coupled neurons in the presence of noise and heterogeneities. *Journal of Computational Neuroscience*, 26(3), 369–392.
- Ozeki, H., Finn, I. M., Schaffer, E. S., Miller, K. D., & Ferster, D. (2009). Inhibitory stabilization of the cortical network underlies visual surround suppression. *Neuron*, 62(4), 578–592.
- Paik, S.-B., & Glaser, D. A. (2010). Synaptic plasticity controls sensory responses through frequency-dependent gamma oscillation resonance. *PLoS Comput. Biol.*, 6(9), e1000927.
- Pollina, B., Benardete, D., & Noonburg, V. W. (2003). A periodically forced Wilson-Cowan system. *SIAM Journal on Applied Mathematics*, 63(5), 1585.
- Ray, S., & Maunsell, J.H.R. (2011). Different origins of gamma rhythm and high-gamma activity in macaque visual Cortex. *PLoS Biology*, 9(4), e1000610.
- Roxin, A., Brunel, N., & Hansel, D. (2005). Role of delays in shaping spatiotemporal dynamics of neuronal activity in large networks. *Physical Review Letters*, 94(23).
- Rubin, D., Van Hooser, S., & Miller, K. (2015). The stabilized supralinear network: A unifying circuit motif underlying multi-input integration in sensory cortex. *Neuron*, 85(2), 402–417.
- Rule, M., Stoffregen, M., & Ermentrout, B. (2011). A model for the origin and properties of flicker-induced geometric phosphenes. *PLoS Comput. Biol.*, 7(9), e1002158.
- Saleh, K., & Wagnere, F.O.O. (2010). Semi-global analysis of periodic and quasi-periodic normal-internal k: 1 and k: 2 resonances. *Nonlinearity*, 23(9), 2219.
- Schilder, F., Osinga, H. M., & Vogt, W. (2005). Continuation of quasi-periodic invariant tori. *SIAM Journal on Applied Dynamical Systems*, 4(3), 459–488.
- Sejnowski, T. J., & Paulsen, O. (2006). Network oscillations: Emerging computational principles. *Journal of Neuroscience*, 26(6), 1673–1676.
- Spiegler, A., Knösche, T. R., Schwab, K., Haueisen, J., & Atay, F. M. (2011). Modeling brain resonance phenomena using a neural mass model. *PLoS Computational Biology*, 7(12), e1002298.
- Tsodyks, M. V., Skaggs, W. E., Sejnowski, T. J., & McNaughton, B. L. (1997). Paradoxical effects of external modulation of inhibitory interneurons. *Journal of neuroscience*, 17(11), 4382–4388.
- Vierling-Claassen, D., & Kopell, N. (2009). The dynamics of a periodically forced cortical microcircuit, with an application to schizophrenia. *SIAM Journal on Applied Dynamical Systems*, 8(2), 710–733.
- Vierling-Claassen, D., Siekmeier, P., Stufflebeam, S., & Kopell, N. (2008). Modeling GABA alterations in schizophrenia: A link between impaired inhibition and altered gamma and beta range auditory entrainment. *Journal of Neurophysiology*, 99(5), 2656–2671.
- Wedgwood, K. C., Lin, K. K., Thul, R., & Coombes, S. (2013). Phase-amplitude descriptions of neural oscillator models. *Journal of Mathematical Neuroscience*, 3(1), 2.
- Wilson, H. R., & Cowan, J. D. (1972). Excitatory and inhibitory interactions in localized populations of model neurons. *Biophysical Journal*, 12(1), 1.
- Womelsdorf, T., Lima, B., Vinck, M., Oostenveld, R., Singer, W., Neuenschwander, S., & Fries, P. (2012). Orientation selectivity and noise correlation in awake monkey

- area V1 are modulated by the gamma cycle. *Proceedings of the National Academy of Sciences*, 109(11), 4302–4307.
- Wright, B., Alderson-Day, B., Prendergast, G., Bennett, S., Jordan, J., Whitton, C., . . . Green, G. (2012). Gamma activation in young people with autism spectrum disorders and typically-developing controls when viewing emotions on faces. *PLoS ONE*, 7(7), e41326.
- Yamamoto, J., Suh, J., Takeuchi, D., & Tonegawa, S. (2014). Successful execution of working memory linked to synchronized high-frequency gamma oscillations. *Cell*, 157(4), 845–857.
- Zhang, Y., & Golubitsky, M. (2011). Periodically forced hopf bifurcation. *SIAM Journal on Applied Dynamical Systems*, 10(4), 1272.

---

Received August 13, 2014; accepted August 3, 2015.